Flow Turbulence Combust (2013) 90:373–386
DOI 10.1007/s10494-012-9438-4

Joint PDF Closure of Turbulent Premixed Flames

Mathias L. Hack · Patrick Jenny

Received: 27 February 2012 / Accepted: 27 October 2012 / Published online: 7 December 2012

Abstract In this paper, a novel model for turbulent premixed combustion in the corrugated flamelet regime is presented, which is based on transporting a joint probability density function (PDF) of velocity, turbulence frequency and a scalar vector. Due to the high dimensionality of the corresponding sample space, the PDF equation is solved with a Monte-Carlo method, where individual fluid elements are represented by computational particles. Unlike in most other PDF methods, the source term not only describes reaction rates, but accounts for "ignition" of reactive unburnt fluid elements due to propagating embedded quasi laminar flames within a turbulent flame brush. Unperturbed embedded flame structures and a constant laminar flame speed (as expected in the corrugated flamelet regime) are assumed. The probability for an individual particle to "ignite" during a time step is calculated based on an estimate of the mean flame surface density (FSD), latter gets transported by the PDF method. Whereas this model concept has recently been published [21], here, a new model to account for local production and dissipation of the FSD is proposed. The following particle properties are introduced: a flag indicating whether a particle represents the unburnt mixture; a flame residence time, which allows to resolve the embedded quasi laminar flame structure; and a flag indicating whether the flame residence time lies within a specified range. Latter is used to transport the FSD, but to account for flame stretching, curvature effects, collapse and cusp formation, a mixing model for the residence time is employed. The same mixing model also accounts for molecular mixing of the products with a co-flow. To validate the proposed PDF model, simulation results of three piloted methane-air Bunsen flames are compared with experimental data and very good agreement is observed.

Keywords Transported PDF method · Turbulent premixed flame modeling

M. L. Hack (✉) · P. Jenny
Institut of Fluid Dynamics, ETH Zurich, Sonneggstr. 3, 8092 Zurich, Switzerland
e-mail: hack@ifd.mavt.ethz.ch

P. Jenny
e-mail: jenny@ifd.mavt.ethz.ch

1 Introduction

Most combustion applications operate at highly turbulent flow conditions, such that accurate descriptions of turbulence, chemistry and their interaction are crucial for reliable predictions. Whereas for non-premixed combustion various models depend on the mixture fraction, for premixed turbulent combustion no such general approach exists. One existing approach is the model by Bray et al. [1]. In their original version it is assumed that the gas is either unburnt or fully burnt. In the transport equation for an averaged progress variable, turbulent convection and mean source term are unclosed. Although progress has been made in modeling the mean source term, this still is an issue in that context; as well as a general closure for turbulent convection capable of properly accounting for counter-gradient diffusion. Another approach are flamelet models [11] based on the level-set formulation [8]. An iso-surface of a non-reacting scalar G describes the position of the flame front, for which a transport equation is solved. Issues due to counter-gradient diffusion are avoided with this approach and it allows to study instantaneous flame dynamics. It is not straightforward however, to achieve closure for turbulent premixed flames. In [12], the transport equation of the joint PDF of velocity and a progress variable was solved by a Monte-Carlo method for flamelet and distributed combustion. With the help of idealized premixed turbulent flame simulations, they have compared a standard PDF closure with combined reaction-diffusion formulation. Their results confirm the bimodal distribution of the progress variable for fast reactions made in the original BML approach.

Here a new modeling approach for premixed turbulent flames in the corrugated flamelet regime is presented. It has to be mentioned that this approach shares the same concept as [21], however, there is a major difference in the calculation of the mean flame surface density. Whereas in [21], modeling of flame stretching, curvature effects, and collapse and cusp formation are treated consistently with the classical formulation for FSD transport equations by a flame stretch factor, here, these effects are modeled via mixing model for the flame residence time. While the former model is consistent with existing ones at the moment closure level, and thus profits from all the corresponding experience, the latter is closed in a more "ad-hoc", but more robust way. The approach is based on solving a transport equation for the joint PDF of velocity, turbulence frequency and a scalar vector with a hybrid particle/finite volume method [7, 13]. Like in other joint velocity composition PDF methods turbulent convection appears in closed form. The source term describes the rate at which unburnt particles get "ignited" by the embedded propagating quasi laminar flame, i.e. it reflects the coupled fine-scale convection–diffusion–reaction dynamics in the flame. For closure, the particle properties $c^* \in \{0, 1\}$ and $\tau^* \geq 0$ are introduced. Similar as in the BML model, the progress variable c^* is zero, if a particle represents the unburnt gas mixture; otherwise $c^* = 1$. The flame residence time τ^* is zero if $c^* = 0$; else it represents the elapsed time since c^* switched from zero to one. This allows to resolve the embedded quasi laminar flame structure by mapping τ^* onto the space coordinate of a precomputed one dimensional laminar flame profile. To estimate the mean flame surface density $\langle\Sigma\rangle$ and thus the particle "ignition" probability P, the binary indicator function $d(\tau^*) \in \{0, 1\}$ is introduced; it is zero except if $0 \leq \tau_a < \tau^* \leq \tau_a + \tau_d$, where τ_d is a specified small time constant and τ_a defines the flame surface. Flame stretching, curvature effects, collapse and cusp

formation are accounted for by a mixing model for τ^*. Numerical results of three piloted premixed jet flames and comparisons with corresponding experimental data demonstrate the generality and accuracy of this new approach.

In the following section, a general outline of the joint PDF method is presented. Then the closure for combustion is explained, the tabulation procedure is discussed and it is shown how molecular mixing is modeled. Finally, numerical validation studies are presented and conclusions are given.

2 Joint PDF Method

In this section, a brief outline of the PDF modeling framework used here is presented. Let $\widetilde{g}$ be the one-point one-time Eulerian mass-weighted joint PDF of (Favre) fluctuating velocity $\boldsymbol{u} = (u_1, u_2, u_3)^T$, turbulence frequency ω and the scalar vector $\boldsymbol{\Phi} = (\Phi_1, \ldots, \Phi_{N_s})$ (N_s is the number of scalars). The corresponding sample space variables are $\boldsymbol{v} = (v_1, v_2, v_3)^T$ for the fluctuating velocities, θ for the turbulence frequency and $\boldsymbol{\Psi} = (\Psi_1, \ldots, \Psi_{N_s})$ for the scalars. Then, the mass density function (MDF) $\mathcal{G}$ is defined as

$$\mathcal{G}(\boldsymbol{v}, \theta, \boldsymbol{\Psi}, \boldsymbol{x}, t) = \langle \rho \rangle \, (\boldsymbol{\Psi}, \boldsymbol{x}, t) \, \widetilde{g}(\boldsymbol{v}, \theta, \boldsymbol{\Psi}; \boldsymbol{x}, t), \tag{1}$$

where $\langle \rho \rangle$ is the mean density. Here, the first scalar represents the (inert) mixture fraction Z, i.e. $\Phi_1 = Z$, the second scalar the progress variable c and the third one the flame residence time τ. From the Navier-Stokes and scalar conservation equations the transport equation for $\mathcal{G}$ can be derived exactly [13]; it reads

$$\begin{aligned}
&\frac{\partial \mathcal{G}}{\partial t} + \frac{\partial \mathcal{G}\left(\widetilde{U}_j + v_j\right)}{\partial x_j} - \frac{\partial \widetilde{U}_i}{\partial x_j}\frac{\partial \mathcal{G} v_j}{\partial v_i} + \frac{1}{\langle \rho \rangle}\frac{\partial \langle \rho \rangle \widetilde{u_i'' u_j''}}{\partial x_j}\frac{\partial \mathcal{G}}{\partial v_i} \\
&\quad = \frac{\partial}{\partial v_i}\left(\mathcal{G}\left\langle \frac{1}{\rho}\frac{\partial p}{\partial x_i} - \frac{1}{\langle \rho \rangle}\frac{\partial \langle p \rangle}{\partial x_i} - \frac{1}{\rho}\frac{\partial \tau_{ij}}{\partial x_j} + \frac{1}{\langle \rho \rangle}\frac{\partial \langle \tau_{ij} \rangle}{\partial x_j} \middle| \boldsymbol{v}, \theta, \boldsymbol{\Psi} \right\rangle\right) \\
&\qquad - \frac{\partial}{\partial \theta}\left(\mathcal{G}\left\langle \frac{D\omega}{Dt} \middle| \boldsymbol{v}, \theta, \boldsymbol{\Psi} \right\rangle\right) + \frac{\partial}{\partial \Psi_\beta}\left(\mathcal{G}\left\langle \frac{1}{\rho}\frac{\partial J_i^\beta}{\partial x_i} \middle| \boldsymbol{v}, \theta, \boldsymbol{\Psi} \right\rangle\right) - \frac{\partial \mathcal{G} S_\beta}{\partial \Psi_\beta} + \mathcal{S}^c(\mathcal{G}).
\end{aligned} \tag{2}$$

Favre-averaged quantities are denoted as $\widetilde{\cdot}$, Reynolds-averaged quantities as $\langle \cdot \rangle$ and volume weighted conditional expectations as $\langle \cdot | \cdot \rangle$. The variable p means pressure, ρ density, τ_{ij} is the viscous stress tensor, $\boldsymbol{J}^\beta$ is the molecular diffusion flux of scalar β and S_β is the source term of scalar β. Moreover, the source $\mathcal{S}^c$ describes discontinuous evolutions; here in particular transitions (jumps) of $\Phi_2 = c$ from zero to one. In the case of a continuously evolving progress variable $\mathcal{S}^c$ would vanish. Note that the left-hand side of Eq. 2 is closed (below it is explained how $\widetilde{\boldsymbol{U}}$ is provided); the conditional expectations on the right-hand side (rhs) on the other hand require modeling. Here, the simplified Langevin model (SLM) [4] is used to close the first rhs-term and another stochastic model is employed for the turbulence frequency [15] in the second rhs-term. It will become clear later that the molecular diffusion flux in the third rhs-term is non-zero only for the scalars Φ_1 and Φ_3, for which a modified IEM mixing model [20] is devised (see Section 6). The fourth rhs-term is non-zero only for scalar $\Phi_3 = \tau$, i.e. $S_\beta = \delta_{3\beta}\Psi_2$, where $\delta_{\alpha\beta}$ is the Kronecker delta. Therefore

τ (which by definition is zero for $c = 0$) represents the time, which elapsed since c switched from zero to one. The probability for this transition from $c = 0$ to $c = 1$ is the topic of the following two sections.

Note that Eq. 2 is not complete, since $\widetilde{\boldsymbol{U}}$ cannot be extracted from the MDF $\mathcal{G}$. Therefore, simultaneously to the modeled version of Eq. 2, the Reynolds averaged Navier-Stokes (RANS) equations are solved to provide the mean velocity. Vice versa, the unclosed terms in the RANS equations are obtained from $\mathcal{G}$. For the RANS equations a finite volume solver is employed and due to the high dimensionality of the sample space a Monte Carlo method is used to solve Eq. 2. In the Monte Carlo method Lagrangian particles consistently evolve in the $\boldsymbol{v}$-θ-$\boldsymbol{\Psi}$-space according to stochastic differential equations (SDE), such that the MDF is represented by the particle ensemble density. Such internally consistent hybrid particle/finite volume PDF solution algorithms proved to be much more efficient than stand-alone particle methods; more details are provided in [7].

3 Combustion Modeling Approach

In this section, the general framework of the new combustion model for turbulent premixed combustion in the corrugated flamelet regime is presented [21]. To simplify the explanations, we consider the computational particles in the PDF solution algorithm, which can also be viewed as representative fluid elements. Essential for the proposed modeling approach are the individual particle properties $Z^*, c^* \in \{0, 1\}$ and $\tau^* \geq 0$ representing the mixture fraction, a progress variable and a flame residence time. Moreover, we introduce the function $d(\tau^*)$ (from now on denoted as d^*), which is one for $0 \leq \tau_a < \tau^* \leq \tau_a + \tau_d$, and zero otherwise. The scalars c^* and τ^* are crucial to model the turbulent flame brush; the mixture fraction Z^* on the other hand quantifies the level of molecular mixing between the reaction products and a potential co-flow stream. Next, the roles of these particle properties are further detailed.

The scalar c^* is a flag indicating whether a particle represents the unburnt reactive mixture. In that case $c^* = 0$, else $c^* = 1$. In the case of infinitely thin embedded flames c^* can be interpreted as a normalized temperature; similar as in the BML model [1]. Here, however, the embedded flame structure is not infinitely thin and to account for that, the flame residence time τ^* is useful. As already mentioned, it is non-zero only if $c^* = 1$ and reflects the time which elapsed since c^* switched from zero to one, i.e. since the particle was "reached" by the embedded flame surface (marking the very front of the embedded flame). Since at this point the corrugated flamelet regime is considered, the embedded flame structure and the laminar flame speed s_L are assumed to remain unaffected by the turbulent eddies and can be obtained from precomputed steady laminar 1D flames. Note that for these calculations complex mechanisms can be considered. Now it is straightforward to consistently map τ^* onto the spatial coordinate of that 1D flame and to retrieve mass fractions and temperature via cheap table look-up. More about tabulation and look-up follows in Section 5. A sketch of such a steady laminar premixed flame profile is depicted in Fig. 1, where the temperature varies from T_u in the unburnt mixture to the adiabatic equilibrium temperature T_b on the burnt side. Shown is also the

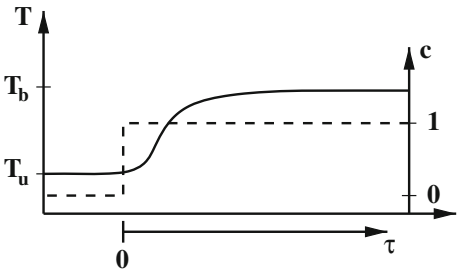

Fig. 1 Sketch of a steady laminar 1D flame profile showing T (solid line), c (dashed line) and τ

variation of c along the flame and the arrow at the bottom indicates the increasing flame residence time τ from left to right where $c = 1$.

The crucial remaining question is: when does the c^* value of a particle switch from zero to one? During a given time step, this occurs with the probability P and a model therefore will be introduced in the following section.

To summarize, during each time step the position $\boldsymbol{X}^*$ of a computational particle evolves according to its individual velocity $\widetilde{\boldsymbol{U}}(\boldsymbol{X}^*) + \boldsymbol{u}^*$, whereas the fluctuating velocity $\boldsymbol{u}^*$ is updated according to the simplified Langevin model (SLM) [4] and the turbulent frequency ω^* by solving another stochastic model equation [15]. Then, if the value of c^* is zero, it is set to one with probability P and if $c^* = 1$, the flame residence time is incremented by the time step size. Now mass fractions and temperature are retrieved from the precomputed tables and a modified IEM model is employed to account for micro-mixing of the flame residence time and the mixture fraction (mixing of products with a potential co-flow stream); details regarding micro-mixing are provided in Section 6.

4 Ignition Probability

In the corrugated flamelet regime, the probability P that a particle is "reached" by the embedded flame during a time step of size Δt is a function of the mean flame surface density $\langle \Sigma \rangle$ and the laminar flame speed s_L (which is assumed constant here). For infinitesimal small time steps one can write $P = F\Delta t$, but to always ensure that $P \in [0, 1]$ the formulation

$$P = 1 - e^{-F\Delta t} \tag{3}$$

is employed; note that F is the ignition probability density. To derive an expression for P, an ergodic statistical fine scale picture of turbulent premixed flames is considered. A sketch of an instantaneous snapshot is depicted in Fig. 2, where the solid line represents the embedded flame front at time t within a volume Ω. The shaded area Ω_d represents the fluid volume, which was "consumed" by this flame front since the time $t - \tau_d$. Note that Ω_d is approximately equal to $A_F l_d$, where A_F is the flame surface area and l_d the average separation distance between the flame front and a fluid element, which was located on the flame front at time $t - \tau_d$. Taking the ensemble average of many such realizations leads to

$$\langle \Omega_d \rangle \approx \langle A_F l_d \rangle = \langle A_F \rangle l_d^{1D} + \langle A_F \delta l_d \rangle \tag{4}$$

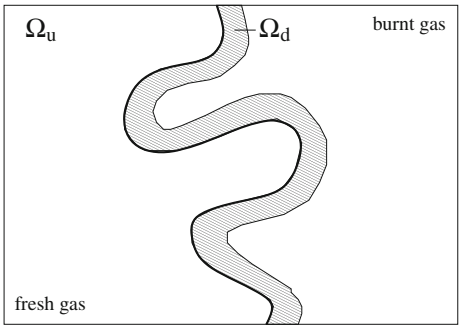

Fig. 2 Sketch of an instantaneous flame surface with the volumes Ω_u (*left*) and Ω_d (*shaded*)

whereas the decomposition $l_d = l_d^{1D} + \delta l_d$ with the corresponding separation distance l_d^{1D} from a laminar 1D flame calculation and the perturbation δl_d is employed. Note that the last term in Eq. 4 requires modeling; e.g. flame stretching results in negative values. For fix τ_d one now can write

$$\langle A_F \rangle = \lim_{\tau_d \to 0} \frac{\langle \Omega_d \rangle - \langle A_F \, \delta l_d \rangle}{l_d^{1D}}. \tag{5}$$

With these definitions, the mean flame surface density can be expressed as

$$\langle \Sigma \rangle = \frac{\langle A_F \rangle}{\Omega} = \lim_{\tau_d \to 0} \frac{\langle \Omega_d \rangle - \langle A_F \, \delta l_d \rangle}{l_d^{1D} \Omega}, \tag{6}$$

which requires modeling of $\langle A_F \, \delta l_d \rangle$; note that $\langle \Omega_d \rangle = \langle d \rangle \Omega$ can be calculated in this PDF modeling framework. Thus, from Eq. 6 one obtains the expression

$$\langle \Sigma \rangle \approx \frac{\langle d \rangle}{l_d^{1D}} - \frac{\langle A_F \, \delta l_d \rangle}{l_d^{1D} \Omega}. \tag{7}$$

Without considering that parts of the flame surface may propagate into itself, the probability for an unburnt fluid element to be "reached" by the propagating embedded flame sheet during the next infinitesimal time interval is

$$F dt = \frac{\langle \Sigma \rangle s_L \Omega}{\Omega_u} dt \approx \frac{1}{1 - \langle c \rangle} \left(\langle d \rangle - \frac{\langle A_F \delta l_d \rangle}{\Omega} \right) \frac{s_L}{l_d^{1D}} dt, \tag{8}$$

where $\Omega_u = (1 - \langle c \rangle)\Omega$ is the volume of unburnt gas. Note that the laminar flame speed s_L is assumed to be a function of the unburnt gas composition and temperature only and that expression (8) is only correct, if all particles with $c^* = 0$ have the same density $\rho = \rho_u$, i.e. if the flame sheet marks the very front of the embedded flame where $T \approx T_u$. With this result based on the above assumptions, for small time steps of length Δt, one obtains the expression

$$P \approx 1 - e^{-F \Delta t} \tag{9}$$

for the ignition probability. Here the effect of $\langle A_F \, \delta l_d \rangle$ and that the flame can run into itself is approximately captured by a mixing model for τ; more details are provided in Section 6.

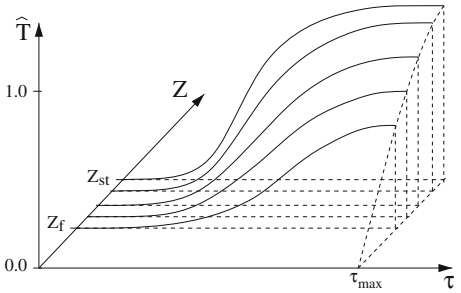

Fig. 3 Sketch of the fuel lean branch of the normalized temperature $\hat{T}$ as a function of Z and τ, where Z_{st} and Z_f are the stoichiometric mixture fraction and the mixture fraction at the fuel lean border of the flamable range, respectively

5 Tabulation

To generalize the combustion model for scenarios where Z of the unburnt reactive mixture varies, multiple laminar 1D flames have to be precomputed and tabulated; i.e. for an adequate number of mixture fraction values in the flammable range. Between these selected Z values, linear interpolation is applied. Outside the flammable range, diffusion dominates and therefore the species mass fractions and temperature are linearly interpolated between the corresponding mixture fraction values. In general, the current model can easily be extended to include fuel rich conditions. But since rich conditions do not occur within the considered flames (flames F1–F3), the stoichiometric-to-rich branch has been omitted in the present description. A sketch of the lean branch of the resulting temperature manifold, i.e. of $T_m(Z, \tau)$, is depicted in Fig. 3. The temperature, and similarly also species mass fractions, can be tabulated as functions of mixture fraction and flame residence time and thus can be retrieved during PDF simulations by simple and cheap look-up operations.

These precomputed tables have some similarities with the ones used in the flamelet generated manifolds (FGM) method [19] or in the flame prolongation of the ILDM method (FPI) [3]. There however, different "control variables" are employed.

6 Molecular Mixing

For the closure of the third rhs-term in Eq. 2, which here affects the Z^* and τ^* values of the computational particles, a variety of micro-mixing models have been devised in the past [6, 10, 18, 20]. In the context of the proposed PDF method, the interaction by exchange with the mean (IEM) model is employed to account for molecular mixing of mixture fraction and temperature. Then, under the assumption that the temperature must lie on the manifold $T_m(Z, \tau)$ and since it is a monotonous function of both Z and τ, it is straight forward to determine the new pair (Z^*, τ^*) from the new values of Z^* and T^*, i.e. after the mixing model has been applied for Z^* and T^*, the mapping $(Z^*, T^*) \rightarrow (Z^*, \tau^*)$ is applied. Note that a one to one mapping of the flame residence time on the precomputed laminar 1D flame only holds in the absence of mixing with a coflow. Therefore, the mapping employed in our work includes the mixture fraction. Note that changing the statistics of τ^* influences the local values of $\langle d \rangle$ and thus also the estimated mean flame surface density as well as the ignition probability. It is questionable, however, whether a mixing model designed for inert scalars like mixture fractions can directly be employed to

describe the effect on τ^*. With this ad-hoc ansatz for flame surface production and dissipation, best results have been achieved with a mechanical-to-scalar time scale ratio of 8. Note that here mixing of τ is motivated primarily to account for flame stretching, curvature effects, collapse and cusp formation, and secondary to account for mixing between products and co-flow. This is a different motivation than in other combustion modeling approaches, where the mechanical-to-scalar time scale ratio had to be adjusted for reactive flows, since some scalar gradients are affected by chemistry. Lindstedt and Vaos [9] investigated the influence of varying C_Φ in the range [2.0, 8.0] for a turbulent premixed combustion model based on a transported joint composition PDF method with a reduced chemical reaction scheme. Stöllinger and Heinz [17] showed good agreement of a piloted premixed burner with a value of $C_\phi = 12.0$; also within a joint composition PDF framework combined with a skeletal mechanism. More recently, Rowinski and Pope [14] presented a detailed study of C_ϕ and concluded that increasing C_ϕ improves the prediction of the flame temperature, whereas a value of approximately 2.0 is most appropriate for inert scalars like the mixture fraction.

7 Results

For validation, numerical calculations for three axisymmetric premixed piloted bunsen flames [2] were performed. Each of these flames has three inflow streams, i.e. an unburnt reactive jet encircled by a hot pilot, both surrounded by a slow ambient air co-flow. The jet bulk velocities are $U_0 = 30$ m/s (flame F3), $U_0 = 50$ m/s (flame F2) and $U_0 = 65$ m/s (flame F1), and the reference turbulent kinetic energies are $k_0 = 3.82$ m^2/s^2, $k_0 = 10.8$ m^2/s^2 and $k_0 = 12.7$ m^2/s^2, respectively. The adiabatic temperature of the fully burnt mixture is $T_b = 2248$ K and that of the unburnt jet stream and the co-flow is $T_u = 298$ K. The measurement errors are estimated to be less than 1 % for the mean velocity and to be less than 10 % for the mean temperature. Profiles at the jet inflow of mean and root mean square (rms) velocities $\widetilde{U}_1$ and u_1^{rms}, respectively, are directly adopted from [2] and the estimation $\widetilde{u_1 u_2} \approx 0.5 u_1^{\mathrm{rms}} u_2^{\mathrm{rms}}$ is used for the velocity covariance (subscripts 1 and 2 indicate axial and radial components, respectively). The turbulence frequency ω at the jet inflow is set proportional to $(\widetilde{u_i u_i}/3)^{0.5}/D$, where $D = 0.012$ m is the jet diameter. Pilot and co-flow have uniform mean velocities, i.e. 1.3 m/s in the hot pilot, 1.0 m/s in the cold pilot and 0.5 m/s in the co-flow. The rms-velocities are $u_1 = u_2 = 0.1$ m/s for the pilot and $u_1 = u_2 = 0.05$ m/s for the co-flow. The turbulence frequency for the pilot is 10^3 s^{-1} and 10^2 s^{-1} for the co-flow. From now on it is convenient to consider the following normalized quantities: the normalized mean axial velocity $\hat{\boldsymbol{U}} = \widetilde{\boldsymbol{U}}/U_0$, the normalized turbulent kinetic energy $\hat{k} = \widetilde{k}/k_0$ and the normalized temperature $\hat{T} = (T - T_u)/(T_b - T_u)$. Normalized temperature and mixture fraction are $\hat{T} = 0$ and $Z = 1$ in the jet, $\hat{T} = 0$ and $Z = 0$ in the co-flow, and $\hat{T} = 0.8$ and $Z = Z_p$ such that $\hat{T}_m(Z_p, \tau \to \infty) = 0.8$.

For the simulations presented in this paper, the simplified manifold $\hat{T}_m(Z, \tau) = \hat{T}_{\mathrm{st}}(\tau) Z$ was employed, whereas $\hat{T}_{\mathrm{st}}(\tau)$ is the normalized temperature along the profile of a premixed 1D flame with stoichiometric mixture (Z_{st}). In the manifold, by construction c is one where $0.05 \leq \hat{T}$ and zero otherwise and the function $d(\tau)$

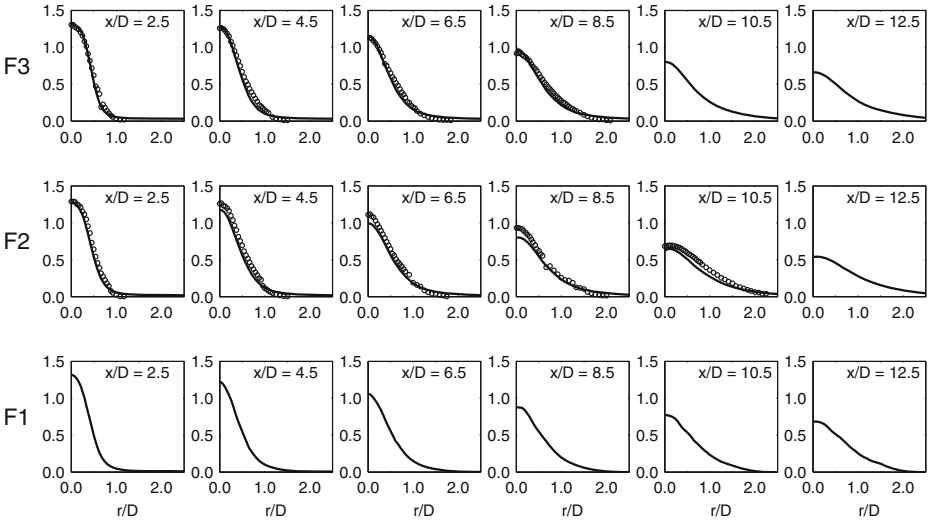

Fig. 4 Radial profiles of the normalized mean downstream velocity $\hat{U}_1$ for the three cold cases at several downstream locations (*circles*: experiment; *solid lines*: numerical simulation)

is chosen such that it is one for $0.2 \leq \hat{T} \leq 0.8$ and zero otherwise; note that this defines $\tau_d = 0.227\ 10^{-3}s$ and $l_d = 0.386\ 10^{-3}$ m. For molecular mixing with the co-flow, C_ϕ values in the range between 2 and 10 were considered. The best agreement for flame F3 was obtained for $C_\Phi = 8$; the same value was then also employed for the simulations of flames F2 and F1.

For the computations a rectangular plane of 0.6 m in axial direction (starting at the nozzle exit) and 0.1 m in radial direction (starting at the symmetry-axis) was considered and a 50×50 non-equidistant grid with an average of 20 computational

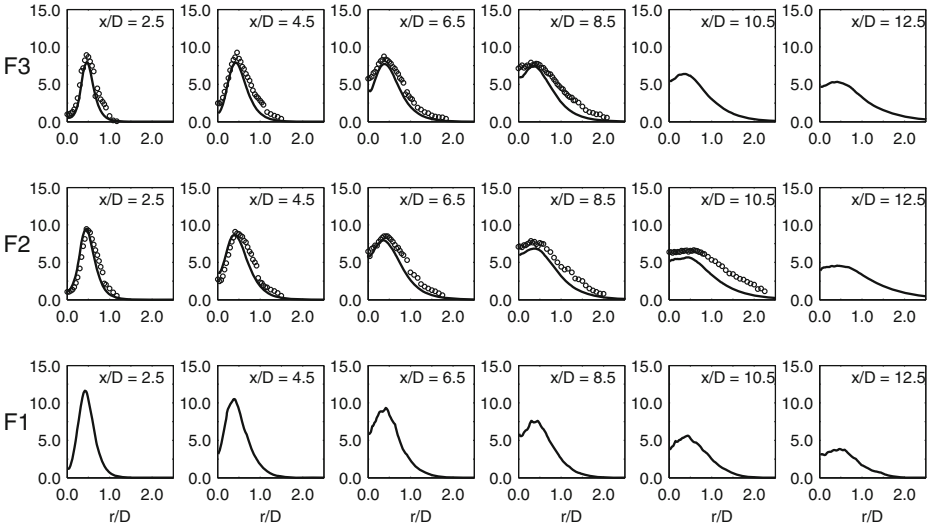

Fig. 5 Radial profiles of the normalized turbulent kinetic energy $\hat{k}$ for the three cold cases at several downstream locations (*circles*: experiment; *solid lines*: numerical simulation)

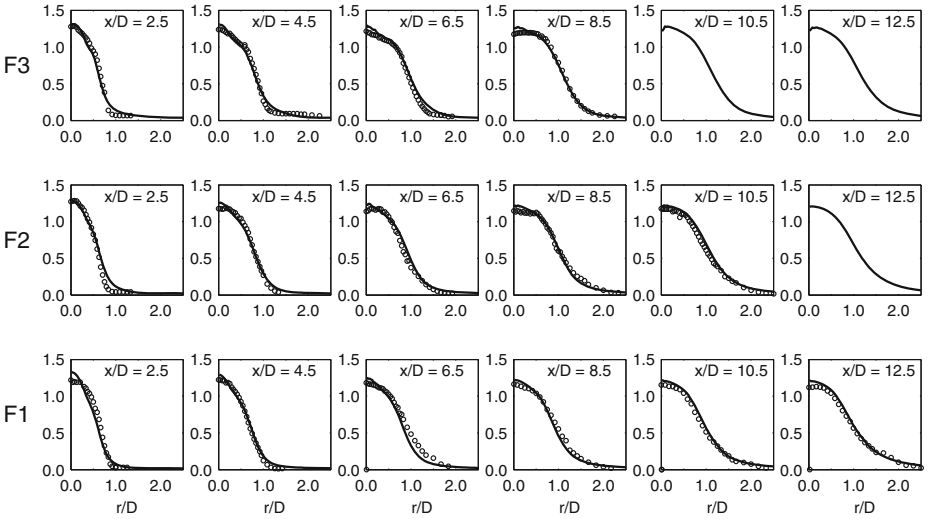

Fig. 6 Radial profiles of the normalized mean downstream velocity $\hat{U}$ for all three flames at several downstream locations (*circles*: experiments; *solid lines*: numerical simulation)

particles per cell was used. To investigate the numerical convergence with respect to grid refinement and particle number, an additional simulation of flame F3 on a 80×80 grid and 30 particles per cell in average was performed; comparison with the result obtained with the 50×50 grid and 20 particles per cell shows very little difference.

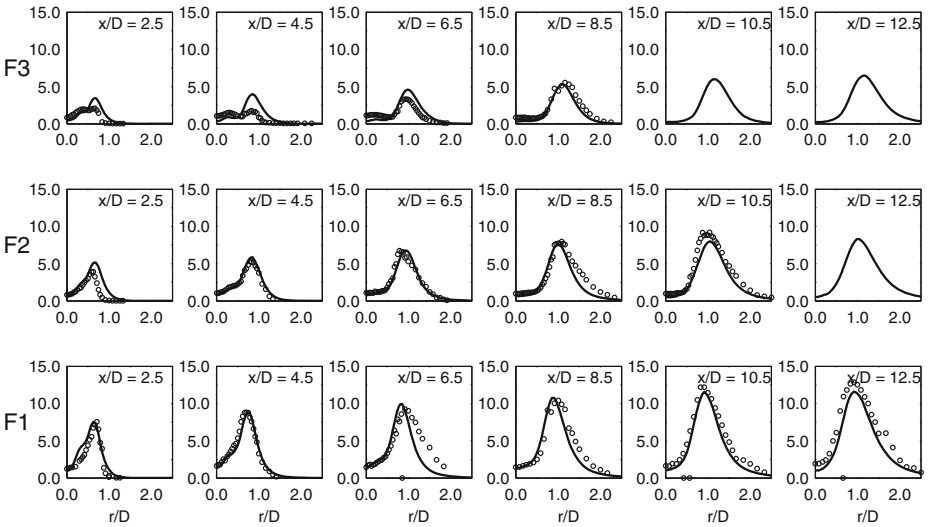

Fig. 7 Radial profiles of the normalized turbulent kinetic energy $\hat{k}$ for all three flames at several downstream locations (*circles*: experiments; *solid lines*: numerical simulation)

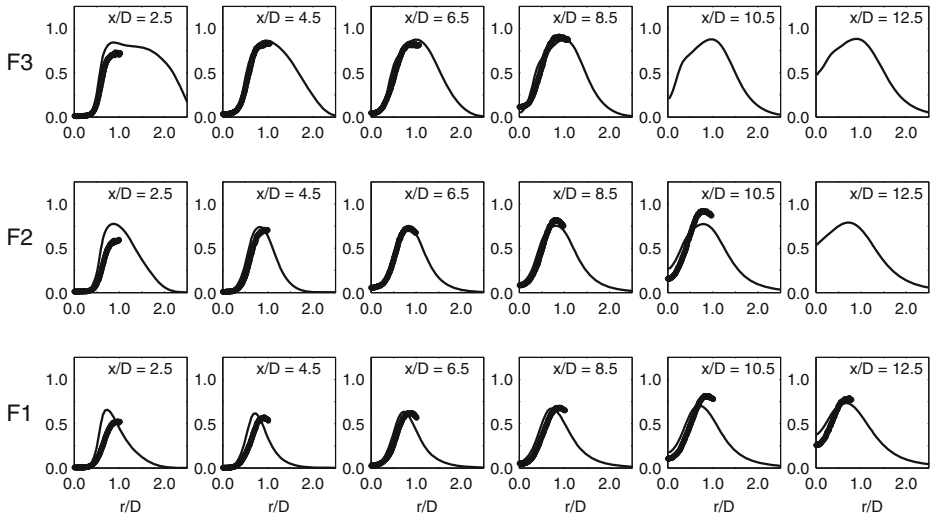

Fig. 8 Radial profiles of the normalized mean temperature $\widetilde{\hat{T}}$ for all three flames at several downstream locations (*circles*: experiment; *solid lines*: numerical simulation)

In Figs. 4 and 5, the normalized mean downstream velocity $\hat{U}_1$ and the normalized turbulent kinetic energy $\hat{k}$ of the non-reactive flow cases are presented. The solid lines represent the simulation results and the circles the experimental data. In general good agreement can be observed for the non-reactive simulation results.

For the reactive flow simulations the same boundary conditions are applied. The normalized mean downstream velocity $\hat{U}_1$ (Fig. 6) and the normalized turbulent kinetic energy $\hat{k}$ (Fig. 7) are predicted very accurately for all three flames. Compared

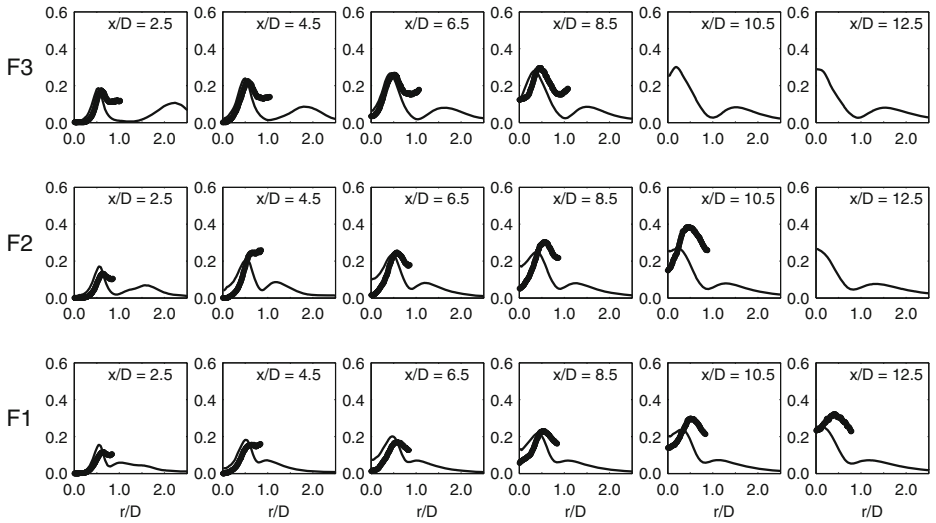

Fig. 9 Radial profiles of the normalized rms-temperature $\hat{T}^{\mathrm{rms}}$ for all three flames at several downstream locations (*circles*: experiment; *solid lines*: numerical simulation)

to the cold cases, the shear layer is shifted outwards due to gas expansion; this effect is captured very well by the presented simulations. In Fig. 8, the normalized mean temperatures are presented. At the axial location $x_1/D = 2.5$ the gradients of $\widetilde{T}$ in the radial profiles are over-predicted; similar over-predictions are also reported in [5, 9, 16], where in [16] it is expected to be caused by the complex interaction of the cold, highly turbulent jet with the hot laminar pilot stream. Note that this effect is not included within the presented model approach. Further downstream, at $x_1/D = 10.5$, the mean temperatures of flames F2 and F1 are under-predicted; otherwise good agreement between simulation and experimental data is observed. Figure 9 shows the normalized rms-temperature $\hat{T}^{\mathrm{rms}}$. For flame F3, the predictions are in good agreement with the experiment; for flames F2 and F1, the predictions are good upstream of $x_1/D = 6.5$; further downstream the model tends to under-predict $\hat{T}^{\mathrm{rms}}$. Compared to the level-set method results [5], the turbulent kinetic energy is forecasted more precisely, whereas the mean velocity and temperature fields are

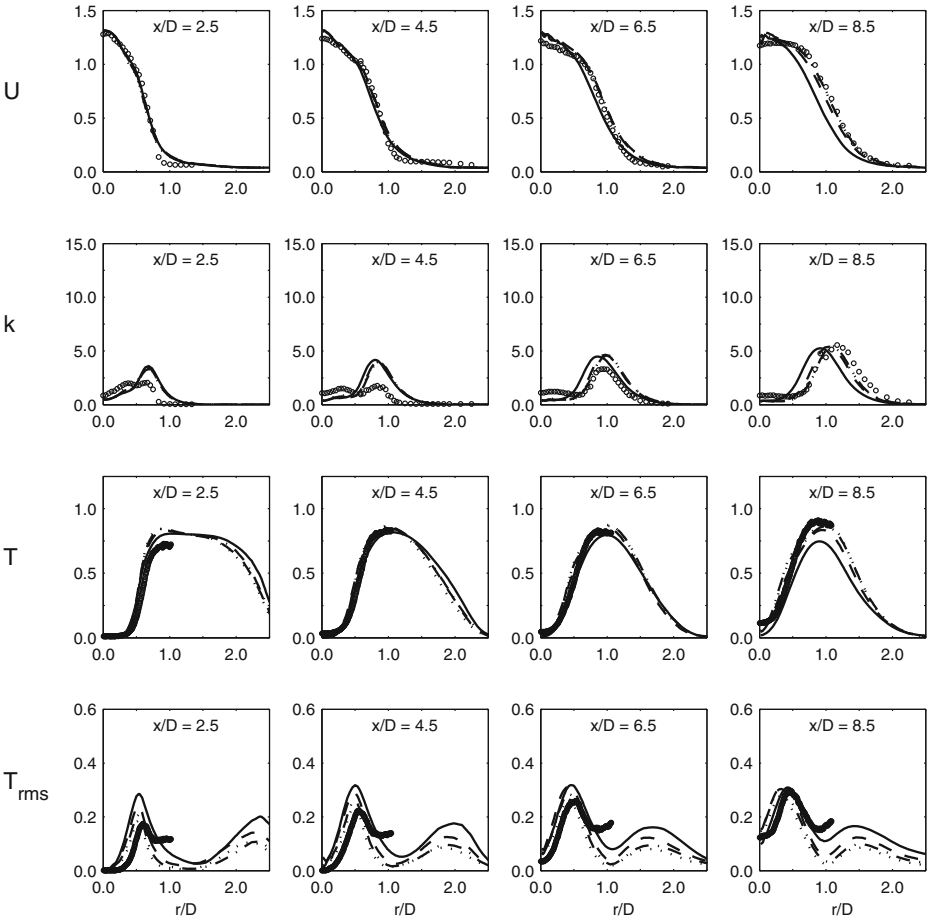

Fig. 10 Radial profiles of the nantities $\hat{U}$, $\hat{k}$, $\widetilde{\hat{T}}$ and $\hat{T}^{\mathrm{rms}}$ for the flame F3 at several downstream locations (experiment: *circles*; numerical simulation: *solid lines* ($C_\phi = 2.0$), *dashed lines* ($C_\phi = 4.0$), *dashed-dotted lines* ($C_\phi = 6.0$) and *dotted lines* ($C_\phi = 8.0$))

comparable. The results are also competitive compared to the detailed chemistry PDF approaches [9, 16] (except for the rms temperatures of flames F1 and F2) at a lower numerical effort, and to the simulation presented in [21]. An important property of the presented model is, however, that very little tuning is required. The only model constant which was systematically adjusted is C_ϕ, and the results are very insensitive to quite large variations as shown in the following.

In Fig. 10, simulation results for flame F3 are presented, where the influence of the mechanical-to-scalar time scale ratio was investigated, i.e. simulations with $C_\phi = 2.0$, $C_\phi = 4.0$, $C_\phi = 6.0$ and $C_\phi = 8.0$ were performed. For $C_\phi = 2.0$, the mean temperature at $x_1/D = 8.5$ is under-predicted. On the other hand, the rms-temperature is over-predicted for positions upstream of $x_1/D = 8.5$. The best general agreement was found for $C_\phi = 8$. It has to be pointed out that the results are very insensitive to quite large variations in the mechanical-to-scalar time scale ratio, which is in huge contrast to previous works.

Before this section is concluded it has to be emphasized that only flame F3 is operated in the corrugated flamelet regime, for which the modeling assumptions are rigorous. Flames F2 and F1 are subject to the thin reaction zone regime and to a small extent even to the broken flamelet regime, where the assumption of unperturbed embedded laminar flame structures is violated, i.e. the enhanced scalar mixing caused by eddies entering the preheat zone is not captured by the presented approach.

8 Conclusion

A novel model for turbulent premixed combustion is presented. The modeled transport equation for the joint PDF of velocity, turbulence frequency, mixture fraction, a binary progress variable and a flame residence time is solved with a hybrid particle/finite volume solution algorithm. Besides other advantages, such joint velocity-scalar PDF methods are not subject to counter gradient diffusion, since turbulent convection appears in closed form.

During a time step, a computational particle representing reactive unburnt mixture is "reached" by the embedded propagating flame surface with the "ignition" probability P, which is a function of the flame surface density. In the proposed joint PDF framework the flame surface density is transported, whereas effects of flame stretching, curvature, collapse and cusp formation have to be modeled. Whereas in [21], modeling of these effects is treated consistently with the classical formulation for FSD transport equations by a flame stretch factor, here, these effects are modeled via mixing model for the flame residence time. Once "reached" by the embedded flame surface, mass fractions and temperature of a particle are governed by the mixture fraction and the flame residence time and can be retrieved by look-up from precomputed premixed laminar flame tables. To account for molecular mixing between the hot products and the co-flow (and to account for production and dissipation of the flame front), the IEM mixing model is employed for mixture fraction and temperature; the flame residence time is then obtained via mapping. An important property of the presented model is, however, that very little tuning is required. The only model constant which was systematically adjusted is C_ϕ, and the results are very insensitive to quite large variations. The best results have been achieved with a mechanical-to-scalar time scale ratio of $C_\Phi = 8$.

Numerical validation studies of piloted premixed Bunsen flames show good agreement with the experimental measurements and demonstrate the applicability of the proposed PDF model for the corrugated flamelet regime. Moreover, the results are also competitive compared to detailed chemistry PDF approaches at a lower numerical effort, except for the rms temperatures. However, more research is required to extend this approach to the thin reaction zone regime and the broken flamelet regime, since the current modeling assumptions are not valid there.

References

1. Bray, K., Moss, J.: A unified statistical model of the premixed turbulent flame. Acta Astronaut. **4**(3–4), 291–319 (1977)
2. Chen, Y.C., Peters, N., Schneemann, G.A., Wruck, N., Renz, U., Mansour, M.S.: The detailed flame structure of highly stretched turbulent premixed methane-air flames. Combust. Flame **107**(3), 223–226 (1996)
3. Gicquel, O., Darabiha, N., Thévenin, D.: Liminar premixed hydrogen/air counterflow flame simulations using flame prolongation of ildm with differential diffusion. Symp. (Int.) Combus. **28**(2), 1901–1908 (2000)
4. Haworth, D.C., Pope, S.B.: A generalized langevin model for turbulent flows. Phys. Fluids **29**(2), 387–405 (1986)
5. Herrmann, M.: Numerical simulation of turbulent bunsen flames with a level set flamelet model. Combust. Flame **145**(1–2), 357–375 (2006)
6. Janicka, J., Kolbe, W., Kollmann., W.: Closure of the transport-equation for the probability density-function of turbulent scalar fields. J. Non-Equilib. Thermodyn. **4**, 47–66 (1979)
7. Jenny, P., Pope, S.B., Muradoglu, M., Caughey, D.A.: A hybrid algorithm for the joint PDF equation of turbulent reactive flows. J. Comput. Phys. **166**, 218–252 (2001)
8. Kerstein, A.R., Ashurst, W.T., Williams, F.A.: Field equation for interface propagation in an unsteady homogeneous flow field. Phys. Rev. A **37**(7), 2728–2731 (1988)
9. Lindstedt, R., Vaos, E.: Transported pdf modeling of high-reynolds-number premixed turbulent flames. Combust. Flame **145**(1–2), 495–511 (2006)
10. Meyer, D.W., Jenny, P.: A mixing model for turbulent flows based on parameterized scalar profiles. Phys. Fluids **18**(3), 035105 (2006)
11. Peters, N.: Laminar flamelet concepts in turbulent combustion. Proc. Combust. Inst. **21**(1), 1231–1250 (1986)
12. Pope, S., Anand, M.: Flamelet and distributed combustion in premixed turbulent flames. Symp. (Int.) Combust. **20**(1), 403–410 (1985)
13. Pope, S.B.: Pdf methods for turbulent reactive flows. Pror. Energy Combust. Sci. **11**(2), 119–192 (1985)
14. Rowinski, D.H., Pope, S.B.: Pdf calculations of piloted premixed jet flames. Combust. Theory Model. **15**(2), 245–266 (2011)
15. Slooten, P.R.V., Jayesh, Pope, S.B.: Advances in pdf modeling for inhomogeneous turbulent flows. Phys. Fluids **10**(1), 246–265 (1998)
16. Stoellinger, M., Heinz, S.: Pdf modeling and simulation of premixed turbulent combustion. Monte Carlo Methods Appl. **14**(4), 343–377 (2008)
17. Stoellinger, M., Heinz, S.: Evaluation of scalar mixing and time scale models in pdf simulations of a turbulent premixed flame. Combust. Flame **157**(9), 1671–1685 (2010)
18. Subramaniam, S., Pope, S.B.: A mixing model for turbulent reactive flows based on euclidean minimum spanning trees. Combust. Flame **115**(4), 487–514 (1998)
19. Van Oijen, J., De Goey, L.: Modelling of premixed laminar flames using flamelet-generated manifolds. Combust. Sci. Technol. **161**(1), 113–137 (2000)
20. Villermaux, J., Devillon, J.: Représentation de la coalesence et de la redispersion des domaines de ségrégation dans un fluide par un modèle d'interaction phénoménologique. In: Proceedings of the Second International Symposium on Chemical Reaction Engineering, pp. 1–13. Elsevier, New York (1972)
21. Zoller, B.T., Hack, M.L., Jenny, P.: A pdf combustion model for turbulent premixed flames. Proc. Combust. Inst. (2012). doi:10.1016/j.proci.2012.05.053